Bioelectrochemistry 104 (2015) 51–57

Contents lists available at ScienceDirect

Bioelectrochemistry

journal homepage: www.elsevier.com/locate/bioelechem

A carbon nanotube/poly [Ni-(Protoporphyrin IX)] composite for amperometric detection of long chain aliphatic amines

Romina Carballo [1], Ana L. Rinaldi, Paula C. Dabas, Irene N. Rezzano *,[1]

IQUIFIB, National Research Council (CONICET), Faculty of Pharmacy and Biochemistry, University of Buenos Aires, Junin 956, CP 1113 Buenos Aires, Argentina

ARTICLE INFO

Article history:
Received 10 November 2014
Received in revised form 19 March 2015
Accepted 22 March 2015
Available online 25 March 2015

Keywords:
Poly [Ni-Protoporphyrin]
MWCNT
Hybrid material
Aliphatic amines
Amperometric detection

ABSTRACT

Poly [Ni-Protoporphyrin] film (pNiPP), containing multiwall carbon nanotubes (MWCNT) was used to cover a glassy carbon electrode. The hybrid material (pNiPP/MWCNT) successfully combines the permselectivity of pNiPP with the high conductivity of MWCNT.

The modified electrode was used to perform amperometric detection of long chain aliphatic amines (LCAA) in order to prevent the passivation effect of the aliphatic chain. Cyclic voltammetry (CV) and electrochemical impedance spectroscopy (EIS) demonstrated that the pNiPP/MWCNT facilitates the electron transfer reaction. The charge transfer resistance (Rct) values were significantly lower by up to one order of magnitude compared to the bare electrode. Differential pulse polarography (DPP) showed a marked decrease of the overpotential generated by the aliphatic chain. The calibration of the amperometric peak area vs. concentrations of derivatized LCAA exhibits a linear response within the range of 0.018 and 28 μM and correlation coefficient (R^2) higher than 0.999 (n = 5). The quantitation limit of the pNiPP/MWCNT electrode is about 400 times lower than the UV–visible detection. RSD of 7.2%, 5.8%, 2.5% and 2.3% was obtained for concentrations of 0.028, 0.28, 2.8 and 28 μM of ferrocenyl octadecylamine. A solution of sphingosine, 0.23 μM, was exclusively detected with HPLC-ECD with pNiPP/MWCNT electrode.

1. Introduction

In the last years, the development of nanostructured conducting polymers has received great attention because of their unique electronic, optical, and mechanical properties that make them versatile high conductivity materials [1]. In this regard, many electrochemically synthetized composites of conducting polymers and carbon nanotubes have shown better mechanical integrity, and higher electronic and ionic conductivity along with larger electrode specific capacitance [2].

Metalloporphyrins are ubiquitous organometallic compounds with interesting physicochemical properties that have been used in numerous electronic and electrochemical devices [3–5]. Therefore, the interaction between porphyrins and nanotubes becomes a very attractive area of research due to the promising optical and electronic properties of the resulting hybrid nanomaterials. A non-covalent wrapping of carbon nanotubes with porphyrins by condensation of formylporphyrins and pyrenes was reported [6]. The porphyrin ring is bonded to the nanotube wall by Van der Waals forces, and the π–π orbital interaction of the porphyrin ring and graphite surface enables the electronic charge transfer [7]. Polymeric bimetallic Fe(III) and Cu(II) porphyrin films were deposited onto multiwalled carbon nanotubes (MWCNT). The method generates stable and homogeneous dispersion of nanotubes in the polymer, favoring the catalytic reduction of hydrogen peroxide [8].

Also, the electrochemical behavior of electrodes modified with Ni(II) Protoporphyrin films was studied. This film does not show significant catalytic properties but deposited onto a glassy carbon electrode behaves as a permselective conducting film with non-Faradic current response proportional to ion concentration in flow injection analysis [9]. This response resulted highly dependent of the electrode potential, which produces positive charges in the film counterbalanced by the movement of ions.

The structural units of the sphingolipids are long-chain aliphatic amines containing two or three hydroxyl groups and often a distinctive *trans*-double bond. The main component in nature is C18, but there are also small amounts of C16 to C19 dihydroxy bases. Sphingolipids have important roles in membrane and in cell regulation as second messengers for growth and differentiation factors [10]; therefore, the development of sensitive and reliable techniques to achieve the simultaneous quantification of different sphingoid bases is a relevant matter.

The most commonly used method to quantify sphingolipids is HPLC with different detectors (UV–vis, fluorometric, amperometric). These detectors require the presence of chromophoric, fluophoric or redox groups in the analyte which are absent in the aliphatic amines. Several studies focused on the detection of low molecular weight aliphatic

* Corresponding author.
E-mail address: irezzano@ffyb.uba.ar (I.N. Rezzano).
[1] CONICET permanent staff.

http://dx.doi.org/10.1016/j.bioelechem.2015.03.002
1567-5394/

amines, employing a series of aromatic reagents that generate fluorescent [11–14] or chemiluminescent labels [15].

The ferrocene (Fc) molecule is one of the most stable and versatile organometallic compounds and has therefore been used as an electroactive component for the construction of redox molecules with various applications (biosensors [16], electrochemical probes [17] and catalysis [18]). Even though the reduction potential is highly dependent on the electronic nature of the substituents [19], the cyclic voltammetry maintains the reversible ferrocene/ferrocenium ion (Fc/Fc^+) redox peak.

As far as we know, few studies have addressed long chain aliphatic amines derivatized with ferrocene [20] probably because the long chain aliphatic amines not only generate an electrode/solution interface with different electrical properties, but also aggregate and adsorb onto the electrode surface [21]. Thus, the supramolecular structures generate a hydrophobic environment which diminishes the charge transfer process.

In this paper, we explore a hybrid nanomaterial (pNiPP/MWCNT) to perform the amperometric detection of long chain aliphatic amines containing the ferrocenyl unit. The combination of the permselectivity of poly [Ni-(Protoporphyrin IX)] films with the electronic properties of the carbon nanotubes results in a composite that overcomes the passivating effect of aliphatic amines.

2. Experimental

2.1. Materials

Ni-Protoporphyrin IX (NiPP) was prepared according to standard procedure [22].

Tetrabutylammonium perchlorate (TBAP) was obtained by precipitation of a saturated solution of the tetrabutylammonium hydroxide with perchloric acid, twice recrystallized from ethanol, and dried under vacuum. *Caution! Perchlorate salts may be explosive. It should be handled with care and in small amounts.*

Multiwalled carbon nanotubes (MWCNT) (diameter 15 ± 5 nm; length 1–5 μm) were purchased from Nano-Lab and used without further purification.

Ferrocene carboxaldehyde (CHOFc) 98%, ferrocene methanol (FcOH) 97%, sodium borohydride, lithium perchlorate, D-sphingosine (d 18:1) (Sph) and hexadecylamine (HDA) 98% were of analytical grade (Sigma). Octadecylamine (ODA) was purchased from Fluka. All other reagents were of analytical grade. Deionized water was used for all aqueous solutions. All solutions were filtered through a 0.45 μm nylon membrane (Micron Separations Inc., Westborough, MA, USA) and degassed before use.

2.2. Apparatus

Cyclic voltammetries (CVs) and amperometric detection were performed with a purpose built potentiostat (TEQ-Argentina), with digital signal generator for implementation of different electrochemical techniques. Electrochemical impedance spectra were recorded using a potentiostat TEQ4-Z (TEQ-Argentina) and a frequency response analyzer. Data analysis was performed with the program ZView (Scribner Associates, USA). A glassy carbon working electrode (0.25 cm^2 area), an Ag/AgCl KCl 3 M reference electrode (BAS) and a platinum wire auxiliary electrode were used for voltammetric, differential pulse polarography, and electrochemical impedance experiments. A purpose built Teflon cell was used in impedance measurements.

An HP8452 diode array spectrophotometer and a quartz crystal cell were used to obtain the UV spectra.

The scanning electron micrographs of the polymers were obtained using a Zeiss DSM982 GEMINI SEM with Field Emission Gun (FEG) and operated at 3 kV.

2.3. Electrochemical measurements

All electrochemical experiments were carried out in acetonitrile: methanol (70:30) with 0.1 M $LiClO_4$. The scan rate range in cyclic voltammetric (CV) was 0.001 V s^{-1} to 1 V s^{-1}.

A frequency range of 100 kHz to 0.1 Hz was used for impedance spectroscopic (EIS) measurements. The amplitude of oscillation was set to 10 mV and the working potential to +0.500 V.

Differential pulse polarography (DPP) experiments were carried out using a potential ramp starting at 0.0 V and going up to 1 V in a pulsed manner. The following experimental parameters were employed: potential step = 0.5 mV, pulse width = 0.06 s, pulse amplitude = 50 mV, and pulse period = 0.2 s.

2.4. Preparation of the modified electrodes

The glassy carbon electrode was polished with 0.3 and 0.05 mm diameter alumina particles and finally rinsed with deionized water. One milligram (1 mg) of MWCNT was ultrasonically dispersed in 4 mL of 3 mM NiPP solution before electropolymerization.

The electropolymerization of pNiPP/MWCNT onto the electrodes was carried out in 0.1 M TBAP/CH_2Cl_2 by potential sweep between 0.00 and +1.80 V (vs. Ag/AgCl) at 0.05 V s^{-1}, five cycles. Then, the film was oxidized by cycling between −0.2 and +1.80 V in aqueous 50 mM KH_2PO_4 solution.

After polymerization the resulting solution was centrifuged during 20 min at 3000 *g*. Once the supernatant was discarded, the solid was re-suspended to obtain the UV–vis spectra of the pNiPP/MWCNT.

2.5. HPLC measurements

The HPLC equipment consisted of a Waters 1525 Binary HPLC pump, a Rheodyne injection valve (Model 7125) with a 50 μL sample loop, a guard column and a reversed phase column, a flow cell for amperometric detection (BAS), and 2487 Dual k Absorbance detector (Waters).

Separation was achieved using a Luna 5u C18 Phenomenex (150 mm × 4.6 mm i.d., 5 μm particle size); the isocratic mobile phase was acetonitrile:methanol (70:30) with 0.1 M $LiClO_4$ and the flow rate 1.0 mL min^{-1}.

Amperometric detection was performed with a microprocessor controlled electrochemical analyzer. The 7 μL thin layer electrochemical cell consisted of a dual glassy carbon working electrode (7 mm^2 working area), Ag/AgCl reference electrode (BAS), and a stainless steel auxiliary electrode. The measurements were carried out at +0.500 V after allowing the transient current to decay to steady state before analysis.

UV detection was performed at 272 nm.

2.6. Preparation and quantification of standard solutions

Ferrocenyl derivatives, FcODA, FcHDA and FcSph, were synthesized and characterized according to the procedure described in the supplementary information.

Standard stock solutions (2.8 mM) of ferrocenyl octadecylamine (FcODA), ferrocenyl hexadecylamine (FcHDA), and ferrocenyl sphingosine (FcSph) were prepared by separately dissolving 13.2 mg, 12.8 mg and 14.2 mg of each compound, respectively, in 10 mL of methanol. Working standard solutions (280, 28, 2.8, 1.4, 0.7, 0.35, 0.28, 0.18 and 0.018 μM) were prepared by diluting the standard solution with methanol.

The chromatographic peak areas were employed to quantify each analyte. Linearity, limits of detection (LODs), and limits of quantitation (LOQs) were compared for the three methods employed: HPLC-UV, and HPLC-ECD with and without pNiPP/MWCNT.

The calibration curves were constructed and treated with linear least square regression analysis. The analytical sensitivity (γ), the most adequate parameter to compare different instrumental methods, is calculated as $\gamma = SEN/s_y$, where s_y is a convenient measure of noise

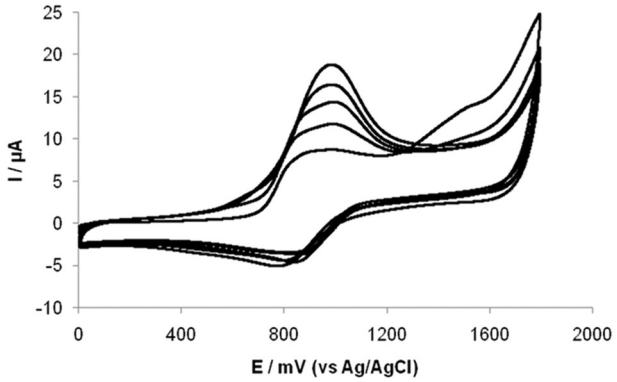

Fig. 1. Voltammograms obtained during electropolymerization of pNiPP/MWCNT onto a glassy carbon electrode. Linear sweep 0.00 to +1.80 V vs. Ag/AgCl at 0.05 V s^{-1}, five cycles.

and SEN is the sensitivity slope of the analytical method [23,24]. The limit of detection (LOD) and the limit of quantitation (LOQ) were determined as $3S_{bl}$/SEN and $10S_{bl}$/SEN, respectively, where S_{bl} is the standard deviation of the blank measurement (n = 10).

3. Results and discussion

3.1. Characterization of the composite

Fig. 1 shows the cyclic voltammograms recorded during the electrochemical polymerization of the NiPP monomer in the presence of MWCNT. The electropolymerization process takes place in the potential range from 0 to 1.8 V (vs. Ag/AgCl) where the monomers polymerize immobilizing the hybrid material (pNiPP/MWCNT) on the electrode surface. Oxidation of Ni^{2+} to Ni^{3+} occurs at +0.900 V, and the corresponding reduction is observed at +0.850 V. This quasi-reversible couple is clearly observed in the presence of nanotubes. The first voltammetric cycle also shows an anodic peak located at +1.50 V (vs. Ag/AgCl) corresponding to radical cation formation, which has been reported during electrooxidation of metalloporphyrins [25].

Table 1
Elemental composition of metals in different parts of pNiPP/MWCNT hybrid nanomaterial.

Element	Weight%	Atomic%
C K	67.15	92.46
O K	4.34	4.48
Cl K	0.37	0.17
K K	0.86	0.36
Ni K	1.22	0.34
Au M	26.06	2.19
Totals	100.00	

Fig. 2A and B shows the in situ EDX with SEM of pNiPP (A) and pNiPP/MWCNT (B) on a gold substrate. In the presence of MWCNT, a fibrous structure can be observed indicative of the incorporation to the polymer matrix. The EDX analysis, employed for elemental identification, confirmed the presence of Ni (Fig. 2C). Taking into account that 1 atom of Ni corresponds to 36 atoms of C of the porphyrin ring, we estimated the amount of porphyrin (12.24%) in the composite as can be seen in Table 1.

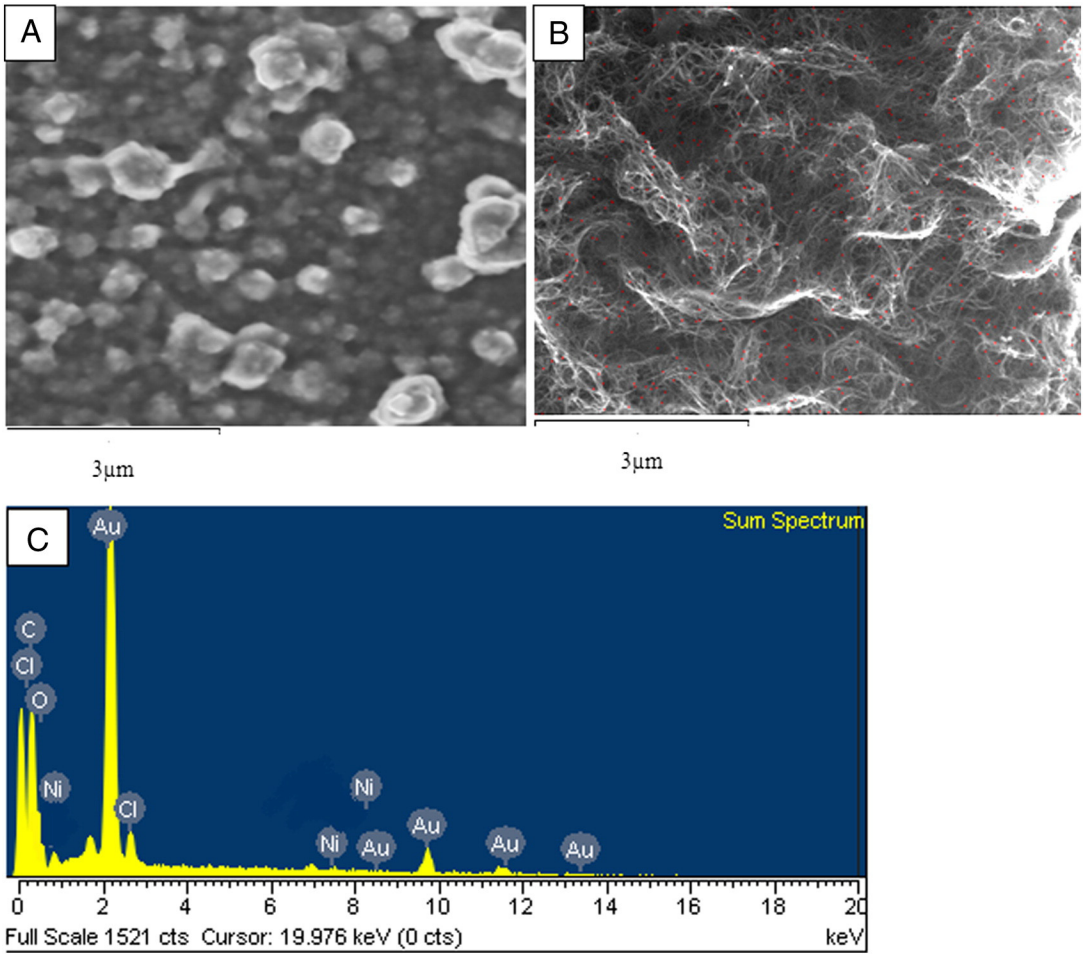

Fig. 2. SEM images of (A) pNiPP and (B) pNiPP/MWCNT with EDS mapping of Ni(II) (red spots) (magnification 5000×). (C) Energy dispersive X-ray analysis exploring the elemental composition of metals in different parts of pNiPP/MWCNT films. (For interpretation of the references to color in this figure legend, the reader is referred to the web version of this article.)

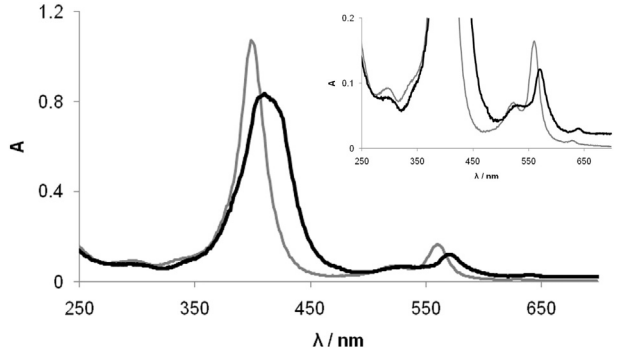

Fig. 3. UV–vis spectra after in dichloromethane after centrifugation at 3000 *g* for 20 min of supernatant pNiPP (gray) and re-suspended pellet pNiPP/MWCNT (black). Inset: amplification of Q bands.

Because the polymerization process continues after the current is shut off [25], different sized bundles of hybrids are expected to be found in solution; the UV–vis reflects this fact by broadening of the typical absorption bands of the porphyrin macrocycle. In order to characterize the interaction between nanotubes and porphyrin, we explored the spectra of the supernatant (mostly pNiPP) and the re-suspended solid (pNiPP/MWCNT) after centrifugation of the electropolymerized solution (see Fig. 3). In both cases the spectra are dominated by the characteristic Q (I_{630}) and Soret (I_{400}) bands. The relative intensity of these bands (I_{400}/I_{630}) shows a dramatic decrease (from 80 to 5) in the hybrid material as well as a red shift (~10 nm) indicating the strong electronic interaction between the porphyrin and the MWCNT [26].

3.2. Electrochemical studies

Fig. 4 shows the cyclic voltammograms of 0.3 mM ferrocene methanol (FcOH) (Fig. 4A) and 0.3 mM ferrocenyl octadecylamine (FcODA) (Fig. 4B) in acetonitrile:methanol (70:30) and 0.1 M $LiClO_4$ with the pNiPP/MWCNT electrode at various potential scan rates. As can be seen, all the experiments exhibit the ferrocene/ferrocenium ion (Fc/Fc^+) redox couple at approximately 0.50 V. The variation of Ep (Fc/Fc^+) as a function of the logarithm of scan rate shows the typical Trumpet plots for FcOH in both electrodes whereas FcODA shows an anomalous behavior with the difference between oxidation and reduction potentials decreasing with increasing scan rate (supplementary information). This result corresponds to a non-homogeneous redox potential resulting from species both in solution and adsorbed to the hybrid composite.

In the case of semi-infinite diffusion, the peak current, ip, in the CV can be expressed by the simplified Randles Sevcik equation

$$ip = 2.65 \times 10^5 \times n^{3/2} \times A \times D^{1/2} \times C_0 \times v^{1/2} \quad (1)$$

where n is the number of transferred electrons, A is the surface area of the electrode, D is the diffusion coefficient, C_0 is the concentration of the ferrocenyl derivatives, and v is the scanning rate.

The peak currents were proportional to the square root of the scan rate in the range 0.001–1 V s^{-1}, as shown in the inset of Fig. 4A and B, indicating a diffusion-controlled process with the modified electrode for both analytes.

We used $D = 7 \times 10^{-6}$ cm^2 s^{-1} for FcOH, obtained from reference [27], to calculate the area of the bare and pNiPP/MWCNT electrodes (0.22 and 0.27 cm^2, respectively). In turn, these calculated area values and a $C_0 = 0.3$ mM were introduced in the slope of ip vs. $v^{1/2}$ to calculate the diffusion coefficients of the FcODA in both electrodes. This proceeding demonstrates a significant difference in the diffusion process of FcODA in the nanocomposite ($D = 2.0 \times 10^{-6}$ cm^2 s^{-1}) compared with the bare electrode ($D = 8.4 \times 10^{-8}$ cm^2 s^{-1}). On the other hand, there are no significant differences between the diffusion coefficients of FcOH using either the bare or the modified electrode (inset Fig. 4A).

The two orders of magnitude increase in the diffusion coefficient indicate a faster mass transfer process inside the nanocomposite and can be understood in terms of the hydrophobicity of the porphyrin

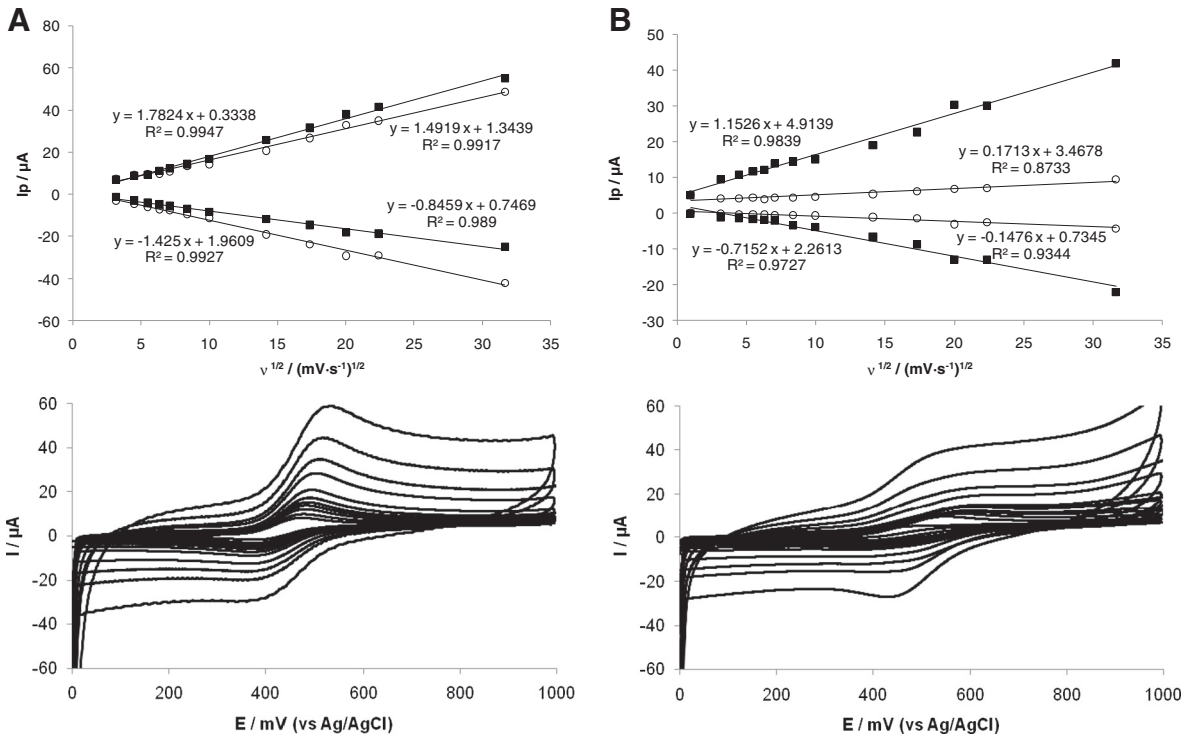

Fig. 4. CVs of pNiPP/MWCNT electrode with 0.3 mM of (A) FcOH and (B) FcODA in acetonitrile:methanol (70:30) and 0.1 M $LiClO_4$ at different scan rates. The scan rates from inner to outer are 0.001, 0.010, 0.020, 0.030, 0.040, 0.050, 0.070, 0.10, 0.20, 0.30, 0.50 and 1.00 V s^{-1}, respectively. Inset: Plot of Ip_a and Ip_c vs. square root of the scan rate for: bare glassy carbon electrode (○) and pNiPP/MWCNT electrode (▪).

film which easily incorporates the aliphatic chain and also facilitates the movement of ions, due to the permselectivity of pNiPP film, in agreement with previous work [9]. To further evaluate the charge transport mechanism, we performed electrochemical impedance spectroscopy (EIS) measurements.

Fig. 5 shows the Nyquist plots for FcODA with both the bare (Fig. 5A) and the modified (pNiPP/MWCNT) electrodes (Fig. 5B). The experimental data are best fitted to the equivalent circuits depicted in Scheme 1, which correspond to the two semicircles observed in Fig. 5A and B. The analysis of the equivalent circuit of FcODA (Scheme 1A) with the bare electrode shows two connected interfaces with a constant phase element (CPE), which replaces the double layer capacitance in the cases of inhomogeneous surfaces [28]. The CPE is in parallel with a resistance (R) in all the cases. It can be seen that there is no Warburg impedance data in this scheme. The parameters CPE_2 and R_3 correspond to the Faradic process in the inner phase. CPE_2 probably results from the insulating effect of the aliphatic chain, which retards the interfacial electron transfer kinetics and increases the electron transfer resistance [29]. R_1 represents the sum of the solution resistance and the resistance of the electrical contacts. CPE_1 and R_2 correspond to the non-Faradic process in the interphase with the bulk solution. This design was used to describe porous electrode surfaces or immobilization of one layer towards another [28–31].

The modified electrode best fits to the model circuit of Scheme 1B, which also contains the corresponding CPE and R components. In this case, we have to highlight the presence of a Warburg impedance element (W) associated with charge transfer resistance. This means that there is mass transfer through the inner layer. As a consequence, the electron transfer resistance in the pNiPP/MWCNT electrode is significantly lower (17,860 Ω) in comparison with the bare electrode (3.3×10^5 Ω).

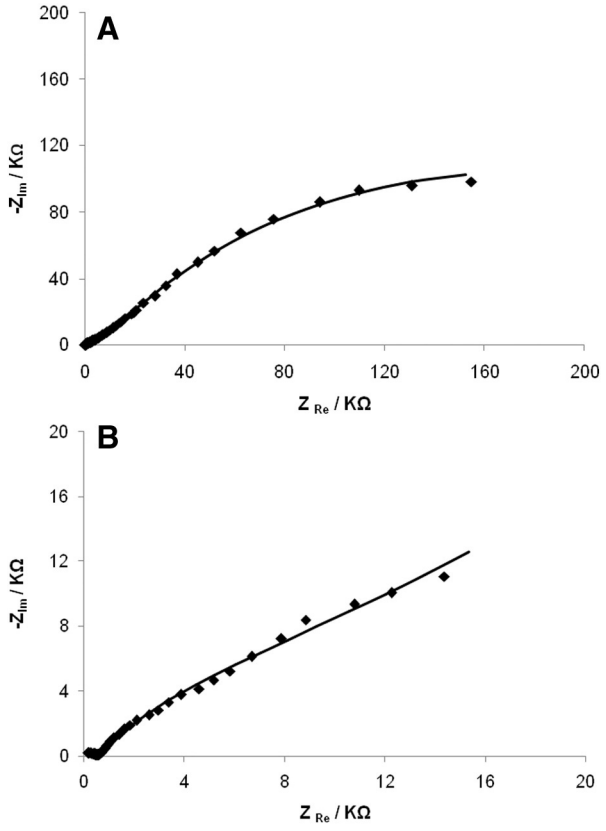

Fig. 5. Nyquist plots resulting from (A) bare glassy carbon electrode and (B) pNiPP/MWCNT electrode. EIS data was obtained in acetonitrile:methanol (70:30) and 0.1 M $LiClO_4$ for 0.15 mM of FcODA at 0.500 V. The frequency range was 100 kHz to 0.1 Hz, the amplitude of oscillation was set to 10 mV. Experimental data (▪), fitted data (—).

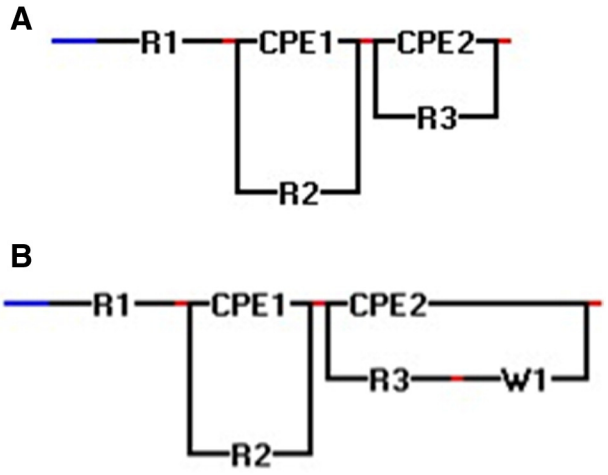

Scheme 1. Scheme of the electrical equivalent circuits proposed for (A) bare glassy carbon electrode and (B) pNiPP/MWCNT electrode. R_1, sum of the solution resistance and the resistance of the electrical contacts; CPE_1 and R_2 correspond to the non-Faradic process in the interphase with the bulk solution; CPE_2 and R_3 correspond to the Faradic process in the inner phase; W_1, the Warburg impedance element.

The impedance analysis of the FcOH measurement does not show differences between the two electrodes, which is in agreement with the cyclic voltammetry conclusions.

We completed the electrochemical analysis performing differential pulse polarography (DPP) of FcODA and FcOH, with and without the

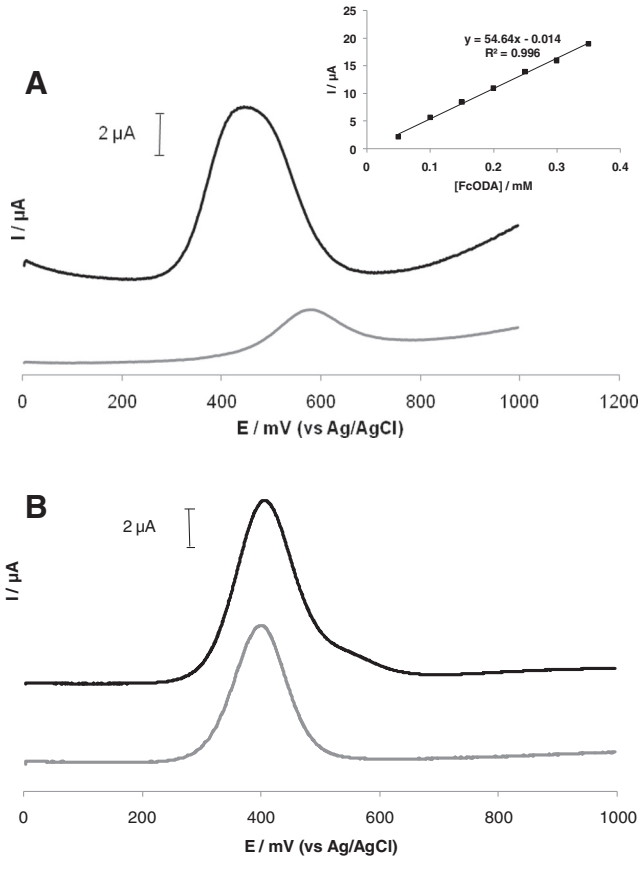

Fig. 6. DPP for bare glassy carbon electrode (gray) and pNiPP/MWCNT electrode (black) in acetonitrile:methanol (70:30) and 0.1 M $LiClO_4$ for the electrooxidation of 0.15 mM of: (A) FcODA. Inset: Plot current vs. FcODA concentrations for pNiPP/MWCNT electrode. (B) FcOH.

pNiPP/MWCNT electrode. These results are shown in Fig. 6. It can be concluded that the composite effectively reduces the overpotential produced by unspecific adsorption of the long aliphatic chains for FcODA oxidation in more than 0.15 V (Fig. 6A). This conclusion is reinforced by DPP results for FcOH, where no changes are observed (Fig. 6B). The DPP experiments show a response proportional to FcODA concentration as can be seen in the inset of Fig. 6A.

Finally, the modified electrode (pNiPP/MWCNT) was explored under hydrodynamic conditions and applied to the amperometric detector of HPLC.

3.3. Chromatographic separation and performance of the analytical method

In order to separate and quantify sphingolipids of different chain-lengths, we performed the chromatographic separation of a mixture of very similar ferrocenyl derivatives, FcHDA, FcODA and FcSph (Fig. 7). The optimization of resolution and rapidness was accomplished by studying different mobile phases and flow rates. The optimum separation was obtained with C18 packed column, acetonitrile:methanol (70:30) with 0.1 M $LiClO_4$ and 1.0 mL min^{-1}.

The performance of the method was defined in terms of linear range, analytical sensitivity, detection limit (LOD), and quantitation limit (LOQ). The calibration of the peak areas vs. concentrations generated a linear response for FcHDA and FcODA within the range of 0.018 and 28 μM with correlation coefficients (R^2) higher than 0.999 (n = 5). Typical calibration curves showed the regression equations y = 0.279 (±0.005) μC·μM^{-1} × +0.064 (±0.003) μC for FcODA and y = 0.286 (±0.004) μC·μM^{-1} × +0.052 (±0.005) μC for FcHDA. The LOD and LOQ for both derivates were similar and equal to 0.006 and 0.018 μM respectively. These parameters were compared with those obtained with the bare electrode and UV–visible detection (Table 2). The pNiPP/MWCNT modified electrode exhibits a marked decrease of the quantitation limit, about 400 times lower than the UV–visible detection.

The precision of the analytical process was calculated by determining the relative standard deviation (RSD) for repeated injections of solutions containing ferrocenyl octadecylamine and using the same modified electrode. Concentrations 0.028, 0.28, 2.8, and 28 μM of FcODA showed RSD of 7.2%, 5.8%, 2.5%, and 2.3%, respectively (n = 5).

4. Conclusions

The modified electrode with pNiPP/MWCNT film facilitates the movement of ions and charge transfer, compensating the overpotential due to a passivation effect by the aliphatic chain-length. This conclusion was demonstrated by cyclic voltammetry experiments where the peak currents were proportional to the square root of the scan rate in the range 0.001–1 V s^{-1}, indicating a diffusion-controlled process for FcODA. The diffusion coefficients estimated from the slope ip vs. $v^{1/2}$ are significantly higher with the composite. EIS experiments confirmed the presence of a Warburg element, ascribed to the mass transport in the inner interphase for FcODA due to the facilitated diffusion inside the pNiPP/MWCNT. Finally, DPP results show the diminution of the overpotential in 0.15 V.

Long chain aliphatic amines, including sphingosine, have been successfully converted in the ferrocenyl derivatives and efficiently separated and quantified by HPLC with amperometric detection. The most diluted solution of sphingosine (0.23 μM) was only detected with the pNiPP/MWCNT electrode; the bare electrode and UV–vis methods are not sensitive enough to be used in this concentration range.

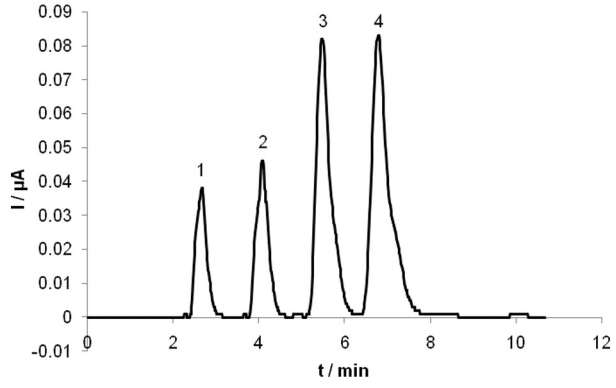

Fig. 7. HPLC-ECD chromatogram of standards and sphingosine ferrocene derivative mixture: peak 1 FcOH (R_t 2.65 min, 0.5 μM), peak 2 FcSph (R_t 4.10 min, 3.5 μM), peak 3 FcHDA (R_t 5.48 min, 6 μM) and peak 4 FcODA (R_t 6.80 min, 6 μM). The mobile phase was acetonitrile:methanol (70:30) and 0.1 M $LiClO_4$ and the flow rate was 1.0 mL min^{-1}. The detection potential was 0.500 V vs. Ag/AgCl using a pNiPP/MWCNT electrode. The injection volume was 50 μL.

Table 2
Comparison of analytical performance for FcODA determination by three methods employed.

	Linear range (μM)	LOD (μM)	LOQ (μM)	Analytical sensitivity (μM^{-1})
HPLC-UV (λ = 272 nm)	7.0–280	2.1	7.0	0.214
HPLC-bare glassy carbon electrode (+0.600 V vs Ag/AgCl)	0.28–28	0.09	0.28	3.14
HPLC-pNiPP/MWCNT (+0.500 V vs Ag/AgCl)	0.018–28	0.006	0.018	3.75

Acknowledgments

Financial support from the University of Buenos Aires (UBACyT 2011-14 0915), ANPCyT (PICT 2011-14) and CONICET (PIP 100076) are gratefully thanked.

Appendix A. Supplementary data

Supplementary data to this article can be found online at http://dx.doi.org/10.1016/j.bioelechem.2015.03.002.

References

[1] C. Li, H. Bai, G. Shi, Conducting polymer nanomaterials: electrosynthesis and applications, Chem. Soc. Rev. 38 (2009) 2397–2409, http://dx.doi.org/10.1039/B816681C.
[2] Ch. Peng, J. Jin, G.Z. Chen, A comparative study on electrochemical co-deposition and capacitance of composite films of conducting polymers and carbon nanotubes, Electrochim. Acta 53 (2007) 525–537, http://dx.doi.org/10.1016/j.electacta.2007.07.004.
[3] D. Wohrle, G. Schnurpfeil, in: K.M. Kadish, K.M. Smith, R. Guilard (Eds.), The Porphyrin Handbook: Phthalocyanines: properties and materials, Academic Press, San Diego, 2003.
[4] D. Holten, D.F. Bocian, J.S. Lindsey, Probing electronic communication in covalently linked multiporphyrin arrays. A Guide to the rational design of molecular photonic devices, Acc. Chem. Res. 35 (2002) 57–69, http://dx.doi.org/10.1021/ar970264z.
[5] M. Jurow, A.E. Schuckman, J.D. Batteas, C.M. Drain, Porphyrins as molecular electronic components of functional devices, Coord. Chem. Rev. 254 (2010) 2297–2310, http://dx.doi.org/10.1016/j.ccr.2010.05.014.
[6] A. Satake, Y. Miyajima, Y. Kobuke, Porphyrin-carbon nanotube composites formed by noncovalent polymer wrapping, Chem. Mater. 17 (2005) 716–724, http://dx.doi.org/10.1021/cm048549a.
[7] G. Almeida Magalhães Sáfar, D. Carvalho da Silva Martins, G. DeFreitas-Silva, J. Santos Rebouças, Y.M. Idemori, A. Righi, Interactions of porphyrins and single walled carbon nanotubes: a fine duet, Synth. Met. 193 (2014) 64–70, http://dx.doi.org/10.1016/j.synthmet.2014.03.026.
[8] M. Hamer, R.R. Carballo, N. Cid, I.N. Rezzano, Study of the electron transfer properties of nanostructured bimetallic films of polymerized porphyrins, Electrochim. Acta 78 (2012) 302–307, http://dx.doi.org/10.1016/j.electacta.2012.05.097.
[9] R. Carballo, V. Campo Dall'Orto, I. Rezzano, Poly[Ni(II)Protoporphyrin IX] modified electrode for amperometric detection of Acetylcholine (Ach) and Choline (Ch), Anal. Lett. 40 (2007) 1962–1971, http://dx.doi.org/10.1080/00032710701484343.
[10] J.S. Norris, Advances in Cancer Research Volume 117, The Role of Sphingolipids in Cancer Development and Therapy, 2013. (and references therein).
[11] Y. Kenji, O. Masanobu, A. Yoshio, Determination of prostaglandin E_2 and the main prostaglandin E metabolite by micro high-performance liquid chromatography using fluorescence derivatization with dansyl hydrazine, J. Pharmacol. Methods 9 (1983) 93–100, http://dx.doi.org/10.1016/0160-5402(83)90001-3.

[12] R. Herraéz-Hernández, C. Cháfer-Pericás, J. Verdú-Andrés, P. Campíns-Falcó, An evaluation of solid phase microextraction for aliphatic amines using derivatization with 9-fluorenylmethyl chloroformate and liquid chromatography, J. Chromatogr. A 1104 (2006) 40–46, http://dx.doi.org/10.1016/j.chroma.2005.11.121.
[13] Dj. Ozama, M.A. Faraj-Zadeh, Determination of low molecular weight aliphatic amines by HPLC in environmental water samples, J. High Resolut. Chromatogr. 19 (1996) 633–638, http://dx.doi.org/10.1002/jhrc.1240191108.
[14] H. Wang, J. Li, X. Liu, H.S. Zhang, *N*-hydroxysuccinimidyl fluorescein-*O*-acetate as a highly fluorescent derivatizing reagent for aliphatic amines in liquid chromatography, Anal. Chim. Acta 423 (2000) 77–83, http://dx.doi.org/10.1016/S0003-2670(00)01097-7.
[15] S. Meseguer Lloret, C. Molins Legua, J. Verdú Andrés, P. Campíns-Falcó, Sensitive determination of aliphatic amines in water by high-performance liquid chromatography with chemiluminescence detection, J. Chromatogr. A 103 (2004) 75–82, http://dx.doi.org/10.1016/j.chroma.2004.02.027.
[16] N.C. Foulds, C.R. Lowe, Immobilization of glucose oxidase in ferrocene-modified pyrrole polymers, Anal. Chem. 60 (1988) 2473–2478, http://dx.doi.org/10.1021/ac00173a008.
[17] I. Tranchant, A.C. Hervé, S. Carlisle, P. Lowe, C.J. Slevin, C. Forssten, J. Dilleen, A.B. Tabor, D.E. Williams, H.C. Hailes, Applications of tailored ferrocenyl molecules as electrochemical probes of biochemical interactions, Bioconjug. Chem. 18 (2007) 199–208, http://dx.doi.org/10.1021/bc060039e.
[18] P. Barbaro, C. Bianchini, G. Giambastiani, S.L. Parisel, Progress in stereoselective catalysis by metal complexes with chiral ferrocenyl phosphines, Coord. Chem. Rev. 248 (2004) 2131–2150, http://dx.doi.org/10.1016/j.ccr.2004.03.022.
[19] M. Emília, N.P.R.A. Silva, A.J.L. Pombeiro, J.J.R. Fraústo da Silva, R. Herrmann, N. Deus, T.J. Castilho, M.F.C.G. Silva, Redox potential and substituent effects at ferrocene derivatives. Estimates of Hammett σp and Taft polar σ substituent constants, J. Organomet. Chem. 421 (1991) 75–90, http://dx.doi.org/10.1016/0022-328X(91)86433-Q.
[20] K. Shimada, T. Oe, M. Tanaka, T. Nambara, Sensitive ferrocene reagents for derivatization of amines for high-performance liquid chromatography with electrochemical detection, J. Chromatogr. B Biomed. Sci. Appl. 487 (1989) 247–255, http://dx.doi.org/10.1016/S0378-4347(00)83034-0.
[21] M. Stadiober, K. Kalcher, G. Raber, C. Neuhold, Anodic stripping voltammetric determination of titanium (IV) using a carbon paste electrode modified with cetyltrimethylammonium, Talanta 43 (1996) 1915–1924, http://dx.doi.org/10.1016/0039-9140(96)01977-7.
[22] D.A. Adler, F.R. Longo, F. Kampas, J. Kim, On the preparation of metalloporphyrins, J. Inorg. Nucl. Chem. 32 (1970) 2443–2445, http://dx.doi.org/10.1016/0022-1902(70)80535-8.
[23] A.C. Olivieri, Analytical figures of merit: from univariate to multiway calibration, Chem. Rev. 114 (2014) 5358–5378, http://dx.doi.org/10.1021/cr400455s.
[24] A.C. Olivieri, N.M. Faber, J. Ferré, R. Boqué, J.H. Kalivas, H. Mark, Uncertainty estimation and figures of merit for multivariate calibration (IUPAC Technical Report), Pure Appl. Chem. 78 (2006) 633–661, http://dx.doi.org/10.1351/pac200678030633.
[25] K.A. Macor, T.G. Spiro, Porphyrin electrode films prepared by electrooxidation of metalloprotoporphyrins, J. Am. Chem. Soc. 105 (1983) 5601–5607, http://dx.doi.org/10.1021/ja00355a012.
[26] G.A.M. Sáfar, H.B. Ribeiro, L.M. Malard, F.O. Plentz, C. Fantini, A.P. Santos, G. de Freitas-Silva, Y.M. Idemori, Optical study of porphyrin-doped carbon nanotubes, Chem. Phys. Lett. 462 (2008) 109–111, http://dx.doi.org/10.1016/j.cplett.2008.07.093.
[27] C. Cannes, F. Kanoufi, A.J. Bard, Cyclic voltammetry and scanning electrochemical microscopy of ferrocenemethanol at monolayer and bilayer-modified gold electrodes, J. Electroanal. Chem. 547 (2003) 83–91, http://dx.doi.org/10.1016/S0022-0728(03)00192-X.
[28] X.-Z. Yuan, C. Song, H. Wang, J. Zhang, Electrochemical Impedance Spectroscopy in PEM Fuel Cells, Springer, 2010.http://dx.doi.org/10.1007/978-1-84882-846-9.
[29] E. Katz, I. Willner, Probing biomolecular interactions at conductive and semiconductive surfaces by impedance spectroscopy: routes to impedimetric immunosensors, DNA-sensors, and enzyme biosensors, Electroanalysis 15 (2003) 913–947, http://dx.doi.org/10.1002/elan.200390114.
[30] R. Ohno, H. Ohnuki, H. Wang, T. Yokoyama, H. Endo, D. Tsuya, M. Izumi, Electrochemical impedance spectroscopy biosensor with interdigitated electrode for detection of human immunoglobulin A, Biosens. Bioelectron. 40 (2013) 422–426, http://dx.doi.org/10.1016/j.bios.2012.07.052.
[31] Z.O. Uyguna, H.D. Ertugrul Uygun, A short footnote: circuit design for faradaic impedimetric sensors and biosensors, Sensors Actuators B 202 (2014) 448–453, http://dx.doi.org/10.1016/j.snb.2014.05.029.